Frontiers of Information Technology & Electronic Engineering
www.jzus.zju.edu.cn; engineering.cae.cn; www.springerlink.com
ISSN 2095-9184 (print); ISSN 2095-9230 (online)
E-mail: jzus@zju.edu.cn

Robust mismatched filtering algorithm for passive bistatic radar using worst-case performance optimization*

Gang CHEN, Jun WANG‡

National Laboratory of Radar Signal Processing, Xidian University, Xi'an 710071, China

E-mail: chengang_xidian@163.com; wangjun@xidian.edu.cn

Received Mar. 19, 2019; Revision accepted Aug. 23, 2019; Crosschecked Apr. 10, 2020

Abstract: Passive bistatic radar detects targets by exploiting available local broadcasters and communication transmissions as illuminators, which are not designed for radar. The signal usually contains a time-varying structure, which may result in high-level range ambiguity sidelobes. Because the mismatched filter is effective in suppressing sidelobes, it can be used in a passive bistatic radar. However, due to the low signal-to-noise ratio in the reference signal, the sidelobe suppression performance seriously degrades in a passive bistatic radar system. To solve this problem, a novel mismatched filtering algorithm is developed using worst-case performance optimization. In this algorithm, the influence of the low energy level in the reference signal is taken into consideration, and a new cost function is built based on worst-case performance optimization. With this optimization, the mismatched filter weights can be obtained by minimizing the total energy of the ambiguity range sidelobes. Quantitative evaluations and simulation results demonstrate that the proposed algorithm can realize sidelobe suppression when there is a low-energy reference signal. Its effectiveness is proved using real data.

Key words: Passive bistatic radar; Range sidelobes; Low signal-to-noise ratio; Mismatched filtering; Worst-case performance optimization

https://doi.org/10.1631/FITEE.1900150 **CLC number:** TN958.97

1 Introduction

Passive bistatic radar (PBR) itself does not transmit electromagnetic waves; it detects targets by exploiting available broadcasters and communication transmissions. Because of the silent working pattern, PBR is not easily disturbed by a hostile radar jammer or attacked by an anti-radiation missile. PBR usually works at a low frequency and covers mainly low-altitude areas, which means that the system can detect stealth and low-altitude targets. There has been emerging interest in exploiting the external non-radar transmitters for PBR. The available transmissions include frequency modulation (FM) (Colone et al., 2013; Martelli et al., 2018), analogue television (ATV) (Zaimbashi, 2017; Chen et al., 2018), digital television (DTV) (Bournaka et al., 2017; Bok, 2018), the Global System for Mobile communication (GSM) (Lu et al., 2007; Tabassum et al, 2016), Long-Term Evolution (LTE) (Salah et al., 2013; Abdullah et al., 2016), wireless fidelity (Wi-Fi) (Milani et al., 2018), and the Global Navigation Satellite System (GNSS) (Clemente and Soraghan, 2014; Ma et al., 2018).

These illuminators usually belong to continuous wave signals, and the signals reflected by the target are weak. Coherent integration is applied to increase the energy level of the weak target echoes and thus to improve the radar detection ability (Lv et al., 2015). Because the transmitted signal is uncontrollable, high-level range sidelobes may exist in the ambiguity

‡ Corresponding author

* Project supported by the National Natural Science Foundation of China (No. 61401526), the 111 Project, China (No. B18039), and the National Key Laboratory of Science Foundation of Science and Technology on Space Microwave, China (No. 614241103030617)

ORCID: Gang CHEN, https://orcid.org/0000-0002-1744-9408; Jun WANG, https://orcid.org/0000-0002-3434-6312

© Zhejiang University and Springer-Verlag GmbH Germany, part of Springer Nature 2020

function, thus degrading the performance of target detection in PBR. Among these non-radar sources, ATV displays typical range sidelobes in PBR. In this study, the ATV signal is discussed in detail; note that this method can be applied to other illuminators of opportunity based on PBR. We choose ATV as the illuminator of opportunity due to its high transmission power and the typical ambiguity function.

ATV signal consists of an audio signal which is frequency-modulated and a video signal which uses an amplitude modulation vestigial sideband as its modulation mode. In this study, the video signal is discussed in detail. For convenience, the video signal is referred to as an ATV signal. The high-level range ambiguity sidelobes caused by the 64-μs line flyback in ATV signals appear every 19.2 km, and are close to the main lobe. These sidelobes have serious effect on obtaining accurate parameters of the targets.

To suppress the range ambiguity sidelobes, a mismatched filtering algorithm proposed by Zrnic et al. (1998) performs well in pulse compression radar and can be used in PBR. In this method, the optimal filter weights are obtained by minimizing the integrated sidelobe level. However, as the energy level of the range ambiguity sidelobes decreases, the energy level in the main lobe decreases simultaneously. To reduce energy loss, a new mismatched filtering algorithm has been proposed by Wang et al. (2011). In this new method, an extra condition is added to restrict the energy loss in the main lobe while maintaining the sidelobe suppression performance. These two mismatched filtering algorithms are aimed at solving the range ambiguity problem, but neither of them discusses the influence of the low signal-to-noise ratio (SNR) in the reference signal. The reference signal is used to obtain the mismatched filter weights. Low SNR in the reference signal will suppress the suppression performance. To solve this low-SNR problem, a robust mismatched filtering algorithm based on worst-case performance optimization is proposed in this study. By considering the error between the observed and the true reference signals, the optimal filter weights of the mismatched filter are obtained by minimizing the total energy of the range ambiguity sidelobes and the energy loss in the main lobe. Because the difference between the observed and the true reference signals is considered, range ambiguity sidelobe suppression can be achieved.

2 Signal model and signal characteristics

The geometry of a PBR system is shown in Fig. 1. Two sets of antennas are located, with the reference antenna pointing toward illuminator's opportunity and the surveillance antenna pointing to the direction that needs to be monitored.

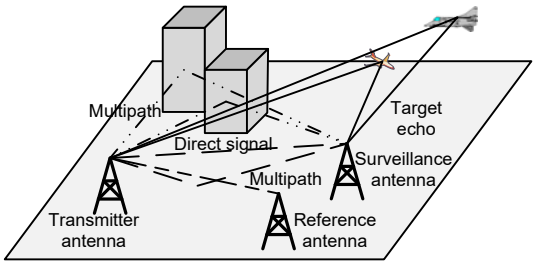

Fig. 1 Passive bistatic radar geometry

The surveillance antenna is used mainly to collect target echoes, but it is inevitably contaminated by the direct signal from the transmitter antenna and by the multipath signal reflected by the ground scatterers. Therefore, the signal collected by the surveillance antenna is expressed as

$$\begin{aligned}\boldsymbol{s}_{\mathrm{sur}}(t) = A_{\mathrm{sur}}\boldsymbol{d}(t) + \sum_{c=1}^{N_c} A_c \boldsymbol{d}(t-\tau_c) \\ + \sum_{k=1}^{N_k} A_k \boldsymbol{d}(t-\tau_k)\mathrm{e}^{\mathrm{j}2\pi f_k t} + \boldsymbol{n}_{\mathrm{sur}}(t),\end{aligned} \tag{1}$$

where $\boldsymbol{d}(t)$ represents the complex envelope of the transmitted signal (The direct signal and the multipath signal comprise the delayed versions of the transmitted signals), A_{sur} the complex amplitude of the direct signal, N_c, A_c, and τ_c the number, complex amplitude, and temporal delay of the cth stationary scatterer (c=1, 2, …, N_c), respectively, N_k, A_k, τ_k, and f_k the number, complex amplitude, temporal delay, and Doppler frequency of the kth target (k=1, 2, …, N_k), respectively, and $\boldsymbol{n}_{\mathrm{sur}}(t)$ the additive noise in the surveillance antenna.

The reference antenna is steered to the transmitter to collect the direct signal as the reference signal for the matched or mismatched filter. Compared with the direct signal, the target echoes and multipath signal received by the reference antenna are usually weak. So, contributions of other reflected signals such as target echoes and multipath signals

can be negligible (Colone et al., 2009). Thus, the signal received by the reference antenna can be expressed as

$$\boldsymbol{s}_{\mathrm{ref}}(t)=A_{\mathrm{ref}}\boldsymbol{d}(t)+\boldsymbol{n}_{\mathrm{ref}}(t), \tag{2}$$

where A_{ref} represents the amplitude of the direct signal and $\boldsymbol{n}_{\mathrm{ref}}(t)$ the additive noise in the reference antenna.

In practical PBR systems, stationary clutterers are stronger than target echoes. To detect the target echoes, clutter cancellation (Garry et al., 2017; Yi et al., 2018) is required. After clutter cancellation, the energy level of the target echoe is lower than that of the thermal noise. A matched filter is applied to raise the energy level of the target echoes, expressed as

$$\boldsymbol{A}(\tau,f)=\int_0^{T_0}\boldsymbol{s}_{\mathrm{sur}}(t)\boldsymbol{s}_{\mathrm{ref}}^*(t-\tau)\mathrm{e}^{-\mathrm{j}2\pi ft}\mathrm{d}t, \tag{3}$$

where T_0 is the integration time, and τ and f are the temporal delay and Doppler frequency, respectively.

Suppose that a digital receiving system is employed to sample the received signals with a sampling frequency f_{s}. This frequency satisfies the Nyquist theorem. Then, the sampled surveillance signal is given by

$$\boldsymbol{s}_{\mathrm{sur}}=\left[s_{\mathrm{sur}}(0),\ s_{\mathrm{sur}}(1),\ \cdots,\ s_{\mathrm{sur}}(N-1)\right]^{\mathrm{T}}, \tag{4}$$

where N denotes the sample number of the signals to be integrated.

Similarly, N samples are obtained by the digital system from the reference signal. Thus, the sampled reference signal is expressed as

$$\boldsymbol{s}_{\mathrm{ref}}=\left[s_{\mathrm{ref}}(0),\ s_{\mathrm{ref}}(1),\ \cdots,\ s_{\mathrm{ref}}(N-1)\right]^{\mathrm{T}}. \tag{5}$$

Then the matched filter is rewritten in a discrete form as

$$\boldsymbol{A}(l,p)=\sum_{i=0}^{N-1}\boldsymbol{s}_{\mathrm{sur}}(i)\boldsymbol{s}_{\mathrm{ref}}^*(i-l)\mathrm{e}^{-\mathrm{j}2\pi pi/N}, \tag{6}$$

where l is the time bin and p the Doppler bin.

To evaluate the performance of the proposed mismatched filtering method, assume that the signals transmitted from an ATV transmission are sampled. The waveform and frequency spectrum of the ATV signal collected by an experimental PBR system are shown in Fig. 2.

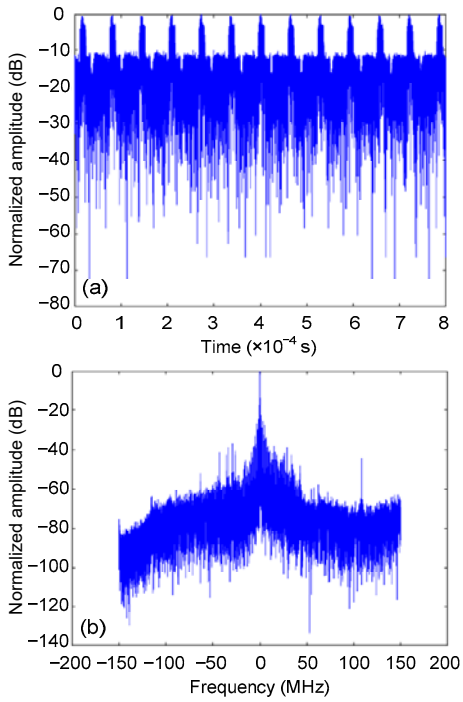

Fig. 2 Characteristics of the analogue television (ATV) signal: (a) waveform; (b) frequency spectrum

Fig. 2a shows that the signal contains high-level correlation of 64 μs. Meanwhile, the frequency spectrum of the ATV signal occupies a bandwidth of 6 MHz (Fig. 2b). However, the main energy of the transmitted ATV signal is distributed in the 400 kHz bandwidth, close to the central carrier frequency. Therefore, it is feasible to use the 400 kHz bandwidth for signal processing in practice, which will surely lower the sampling rate and further reduce the processing time. The frequency spectrum of the 400 kHz bandwidth ATV signal is shown in Fig. 3.

Fig. 3 shows that the frequency spectrum of the signal possesses high-level peaks every 15 625 Hz, corresponding to the 64-μs line flyback of the signal. The 64-μs line flyback will cause range ambiguity sidelobes in the ambiguity function. The ambiguity diagram of the ATV signal is shown in Fig. 4.

From Fig. 4, it can be seen that the outputs of the matched filter contain high-level sidelobes in the range dimension almost as high as the main lobe. These range ambiguity sidelobes have effect on

exacting the range information of the targets. To deal with this problem, a mismatched filtering method was proposed by Wang et al. (2011), which will be introduced in the next section.

3 Mismatched filtering algorithm

The mismatched filtering algorithm based on least squares, proposed by Zrnic et al. (1998), is employed to solve the problem of sidelobes in the range dimension, but the SNR in the main lobe is inevitably reduced. To balance SNR loss and suppression performance, a new mismatched filtering algorithm was proposed by Wang et al. (2011). In this algorithm, the batch version is employed to shorten the computation time. Supposing that $\boldsymbol{s}_{\mathrm{ref}}(k)$ is the sampled and down-converted ATV signal, the optimal mismatched filter weights are obtained by the following cost function:

$$\min_{\boldsymbol{w}} \boldsymbol{J} = (\boldsymbol{w}-\boldsymbol{w}_0)^{\mathrm{H}}(\boldsymbol{w}-\boldsymbol{w}_0) + \sum_{\substack{k=-R \\ k\neq 0}}^{R} c\boldsymbol{w}^{\mathrm{H}}\boldsymbol{S}(k)\boldsymbol{S}^{\mathrm{H}}(k)\boldsymbol{w}, \tag{7}$$

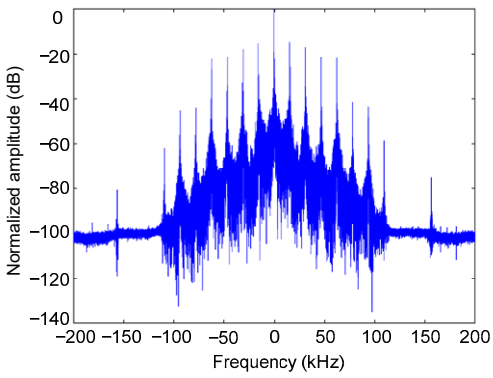

Fig. 3 Spectrum of the 400 kHz bandwidth of the ATV signal

where $\boldsymbol{w}$ represents the mismatched filter weight to be obtained, $\boldsymbol{w}_0$ the matched filter weight which is equal to that of the reference signal, c the weight factor designed to adjust the sidelobe suppression performance and SNR loss in the main lobe, and R the total number of sidelobes to be suppressed. In addition, $\boldsymbol{S}(k)=[s_{\mathrm{ref}}(1+k), s_{\mathrm{ref}}(2+k), \ldots, s_{\mathrm{ref}}(N+k)]$.

The first part on the right-hand side of cost function (7) is related to the SNR loss in the mismatched filter. The SNR loss is contrasted with that of the matched filter. The second part on the right-hand side of cost function (7) represents the total energy of the ambiguity sidelobes in the range dimension. The lower total energy of the range ambiguity sidelobes means a better suppression performance. When the range ambiguity sidelobes are suppressed, the SNR loss will be significant. Thus, a trade-off between the suppression performance and SNR loss is achieved with the use of the weight factor c. The larger the c, the better the suppression performance. Conversely, the less the SNR loss, the smaller the c.

It is easy to prove that problem (7) is a convex one. The optimal solution can be achieved using the following equation:

$$\frac{\partial \boldsymbol{J}}{\partial \boldsymbol{w}^{\mathrm{H}}} = \boldsymbol{w}-\boldsymbol{w}_0 + \sum_k c\boldsymbol{S}(k)\boldsymbol{S}^{\mathrm{H}}(k)\boldsymbol{w} = \boldsymbol{0}. \tag{8}$$

Solving Eq. (8), the optimal solution is written as

$$\boldsymbol{w} = \left(\boldsymbol{I}_N + \sum_k c\boldsymbol{S}(k)\boldsymbol{S}^{\mathrm{H}}(k)\right)^{-1}\boldsymbol{w}_0, \tag{9}$$

where $\boldsymbol{I}_N$ is an identity matrix.

This result has been derived under the assumption that the reference signal is measured with a high SNR. However, this assumption may not always hold; for example, when the reference antenna is distantly

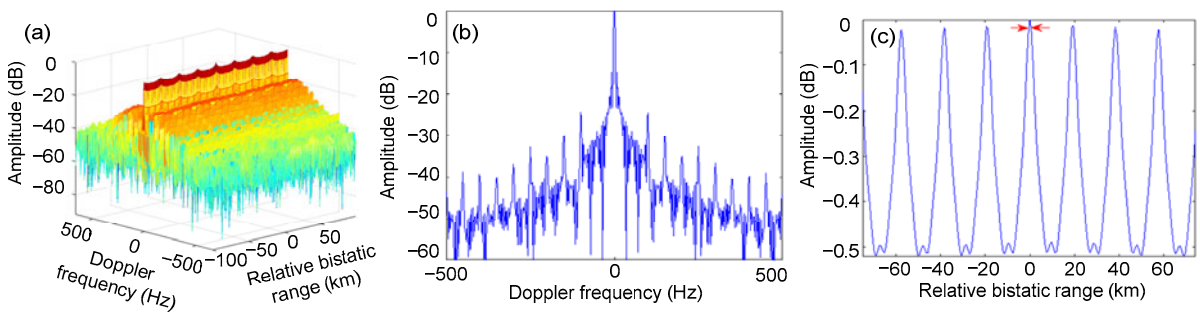

Fig. 4 Matched filter outputs of the ATV signal: (a) two-dimensional range-Doppler frequency results; (b) zero Doppler cut; (c) zero range cut

located or has a low gain, a low SNR reference signal occurs, which will degrade the performance of the mismatched filter. Thus, the algorithm must be improved to obtain a robust solution of the mismatched filter.

4 Robust mismatched filtering algorithm

To solve the problem of low SNR in the reference signal when a mismatched filter is applied, a robust algorithm is proposed in this section. By this robust method, the influence of the low SNR in the reference signal is considered in the optimization problem to improve the suppression performance. For this purpose, a new cost function is designed. By this new method, range ambiguity sidelobes can be suppressed when the SNR of the reference signal is low.

Suppose that $\boldsymbol{s}_{\mathrm{ref}}(k)$ and $\tilde{\boldsymbol{s}}_{\mathrm{ref}}(k)$ are the observed and the true reference signals, respectively. The difference between the true and the observed reference signals is considered in this mismatched filtering method. The error vector $\boldsymbol{e}$ is restrained by an obtained constant number ε, expressed as

$$\left\|\boldsymbol{s}_{\mathrm{ref}}(k)-\tilde{\boldsymbol{s}}_{\mathrm{ref}}(k)\right\|_2=\|\boldsymbol{e}\|_2\le\varepsilon, \tag{10}$$

where $\|\boldsymbol{e}\|_2$ is the norm-2 of the error vector $\boldsymbol{e}$.

The main element of the reference signal is supposed to be the direct signal. Thus, the constant number ε can be obtained through a singular value of the observed reference signal. When the error vector $\boldsymbol{e}$ is restrained by the constant number ε, the observed reference signal $\boldsymbol{s}_{\mathrm{ref}}(k)$ is considered to belong to the set $\boldsymbol{A}(\varepsilon)$, expressed as

$$\boldsymbol{A}(\varepsilon)=\left\{\boldsymbol{a}\,\middle|\,\boldsymbol{a}=\tilde{\boldsymbol{s}}_{\mathrm{ref}}(k)+\boldsymbol{e},\ \|\boldsymbol{e}\|\le\varepsilon\right\}. \tag{11}$$

To obtain a robust solution, ε is required to constrain the vector in $\boldsymbol{A}(\varepsilon)$. Segmenting the one-dimensional reference signal into several parts of a matrix, ε is the singular value of the matrix obtained by singular value decomposition. This constraint ε is added to limit the SNR loss in the main lobe when the mismatched filter is applied, expressed as

$$|\boldsymbol{w}^{\mathrm{H}}\boldsymbol{a}|\ge 1,\ \boldsymbol{a}\in\boldsymbol{A}(\varepsilon). \tag{12}$$

Then, the new cost function applied to the proposed mismatched filtering algorithm is written as

$$\min_{\boldsymbol{w}}\ \sum_k c\boldsymbol{w}^{\mathrm{H}}\boldsymbol{S}(k)\boldsymbol{S}^{\mathrm{H}}(k)\boldsymbol{w}\ \text{ s.t. }\ |\boldsymbol{w}^{\mathrm{H}}\boldsymbol{a}|\ge 1,\ \boldsymbol{a}\in\boldsymbol{A}(\varepsilon), \tag{13}$$

where $\sum_k \boldsymbol{w}^{\mathrm{H}}\boldsymbol{S}(k)\boldsymbol{S}^{\mathrm{H}}(k)\boldsymbol{w}$ is the total energy of the sidelobes in the range dimension. $|\boldsymbol{w}^{\mathrm{H}}\boldsymbol{a}|\ge 1$ is used to limit the SNR loss in the main lobe.

Assuming that $\tilde{\boldsymbol{w}}$ is the optimal solution and satisfies $\chi=\min_{\boldsymbol{a}\in\boldsymbol{A}(\varepsilon)}|\boldsymbol{w}^{\mathrm{H}}\boldsymbol{a}|\ge 1$, there is another filter weight $\hat{\boldsymbol{w}}=\tilde{\boldsymbol{w}}/\chi$ that satisfies

$$\begin{aligned}\sum_k c\tilde{\boldsymbol{w}}^{\mathrm{H}}\boldsymbol{S}(k)\boldsymbol{S}^{\mathrm{H}}(k)\tilde{\boldsymbol{w}}&\ge\sum_k c\hat{\boldsymbol{w}}^{\mathrm{H}}\boldsymbol{S}(k)\boldsymbol{S}^{\mathrm{H}}(k)\hat{\boldsymbol{w}}\\&=\sum_k c\tilde{\boldsymbol{w}}^{\mathrm{H}}\boldsymbol{S}(k)\boldsymbol{S}^{\mathrm{H}}(k)\tilde{\boldsymbol{w}}/\chi^2.\end{aligned} \tag{14}$$

At the same time, the constraint condition is satisfied. Because $\tilde{\boldsymbol{w}}$ is the optimal solution, it can be considered that $\chi=1$. So, $|\boldsymbol{w}^{\mathrm{H}}\boldsymbol{a}|\ge 1$ in Eq. (13) can be transformed into

$$\min_{\boldsymbol{a}\in\boldsymbol{A}(\varepsilon)}|\boldsymbol{w}^{\mathrm{H}}\boldsymbol{a}|=1. \tag{15}$$

According to Vorobyov et al. (2003), Eq. (15) can be transformed into the following form:

$$\left|\boldsymbol{w}^{\mathrm{H}}\boldsymbol{s}_{\mathrm{ref}}(k)\right|\ge\varepsilon\|\boldsymbol{w}\|_2+1. \tag{16}$$

Thus, Eq. (13) can be transformed into the following problem:

$$\min_{\boldsymbol{w}}\sum_k c\boldsymbol{w}^{\mathrm{H}}\boldsymbol{S}(k)\boldsymbol{S}^{\mathrm{H}}(k)\boldsymbol{w}\ \text{ s.t. }\ |\boldsymbol{w}^{\mathrm{H}}\boldsymbol{s}_{\mathrm{ref}}(k)|\ge\varepsilon\|\boldsymbol{w}\|_2+1. \tag{17}$$

According to the principle of rotation invariance in phase (Vorobyov et al., 2003), when $\tilde{\boldsymbol{w}}$ is the optimal solution to cost function (17), $\tilde{\boldsymbol{w}}$ can be rotated in phase while keeping the value of the objective function, so that the value $\boldsymbol{w}^{\mathrm{H}}\boldsymbol{s}_{\mathrm{ref}}(k)$ is a real number. After rotating in phase, $\tilde{\boldsymbol{w}}$ is satisfied with the following equation:

$$\begin{cases}\mathrm{Re}(\boldsymbol{w}^{\mathrm{H}}\boldsymbol{s}_{\mathrm{ref}}(k))>0,\\ \mathrm{Im}(\boldsymbol{w}^{\mathrm{H}}\boldsymbol{s}_{\mathrm{ref}}(k))=0.\end{cases} \tag{18}$$

Then, problem (17) can be transformed into

$$\min_{\boldsymbol{w}}\sum_k c\boldsymbol{w}^{\mathrm{H}}\boldsymbol{S}(k)\boldsymbol{S}^{\mathrm{H}}(k)\boldsymbol{w}\ \text{ s.t. } \boldsymbol{w}^{\mathrm{H}}\boldsymbol{s}_{\mathrm{ref}}(k)\geq\varepsilon\|\boldsymbol{w}\|_2+1. \tag{19}$$

Because problems (13) and (15) are equivalent, the optimization problem (19) can be rewritten as

$$\min_{\boldsymbol{w}}\sum_k c\boldsymbol{w}^{\mathrm{H}}\boldsymbol{S}(k)\boldsymbol{S}^{\mathrm{H}}(k)\boldsymbol{w}\ \text{ s.t. } \boldsymbol{w}^{\mathrm{H}}\boldsymbol{s}_{\mathrm{ref}}(k)-1=\varepsilon\|\boldsymbol{w}\|_2. \tag{20}$$

Square both sides of the constraint condition, and we can obtain

$$\min_{\boldsymbol{w}}\sum_k c\boldsymbol{w}^{\mathrm{H}}\boldsymbol{S}(k)\boldsymbol{S}^{\mathrm{H}}(k)\boldsymbol{w}\ \text{s.t. } [\boldsymbol{w}^{\mathrm{H}}\boldsymbol{s}_{\mathrm{ref}}(k)-1]^2=\varepsilon^2\boldsymbol{w}^{\mathrm{H}}\boldsymbol{w}. \tag{21}$$

This optimization problem can be solved by the Lagrange multiplier method. The Lagrange function of cost function (21) can be expressed as

$$\begin{aligned}L(\boldsymbol{w},\lambda)=&\sum_k c\boldsymbol{w}^{\mathrm{H}}\boldsymbol{S}(k)\boldsymbol{S}^{\mathrm{H}}(k)\boldsymbol{w}-\lambda\Big[\boldsymbol{w}^{\mathrm{H}}\boldsymbol{s}_{\mathrm{ref}}(k)\boldsymbol{s}_{\mathrm{ref}}^{\mathrm{H}}(k)\boldsymbol{w}\\&-\boldsymbol{w}^{\mathrm{H}}\boldsymbol{s}_{\mathrm{ref}}(k)-\boldsymbol{s}_{\mathrm{ref}}^{\mathrm{H}}(k)\boldsymbol{w}+1-\varepsilon^2\boldsymbol{w}^{\mathrm{H}}\boldsymbol{w}\Big].\end{aligned} \tag{22}$$

By solving the conjugate gradient of the Lagrange function of $\boldsymbol{w}$, we can obtain

$$\begin{aligned}\frac{\partial L}{\partial\boldsymbol{w}^{\mathrm{H}}}=&\sum_k c\boldsymbol{S}(k)\boldsymbol{S}^{\mathrm{H}}(k)\boldsymbol{w}-\lambda\Big[\boldsymbol{s}_{\mathrm{ref}}(k)\boldsymbol{s}_{\mathrm{ref}}^{\mathrm{H}}(k)\boldsymbol{w}\\&-\boldsymbol{s}_{\mathrm{ref}}(k)-\varepsilon^2\boldsymbol{w}\Big]=\boldsymbol{0}.\end{aligned} \tag{23}$$

Solving Eq. (23), the optimal solution of the problem can be expressed as

$$\begin{aligned}\boldsymbol{w}=-\lambda\Bigg[&\sum_k c\boldsymbol{S}(k)\boldsymbol{S}^{\mathrm{H}}(k)-\lambda\boldsymbol{s}_{\mathrm{ref}}(k)\boldsymbol{s}_{\mathrm{ref}}^{\mathrm{H}}(k)\\&+\lambda\varepsilon^2\boldsymbol{I}_N\Bigg]^{-1}\boldsymbol{s}_{\mathrm{ref}}(k).\end{aligned} \tag{24}$$

To obtain the optimal solution of the proposed method, λ is a Lagrange multiplier that needs to be further solved. Readers can refer to Vorobyov et al. (2003) and Lorenz and Boyd (2005) to learn how to acquire the value of λ.

In PBR systems, long coherent integration time is required to raise the energy level of the weak target echoes. The length of the mismatched filter is large, and the computation complexities in obtaining the mismatched filter weights are significant. The complex multiplication in solving problem (24) is $O[(2R+1)N^2+N^2(\log N+1)]$, where R is the number of range ambiguity sidelobes to be suppressed and N is the length of the mismatched filter. Usually, solving problem (24) with N (whose value is tens of thousands or more) requires significant calculation.

To decrease the computational cost, the batch version of mismatched filtering was proposed by Wang et al. (2011). Instead of solving problem (24) directly, the batch version segments the mismatched filter weights into $b=N/N_{\mathrm{B}}$ parts, where N_{B} is the length of each batch of mismatched filter weights. Thus, the total mismatched filter weights can be expressed as

$$\boldsymbol{w}=[\boldsymbol{w}_{\mathrm{B}_0}^{\mathrm{T}},\boldsymbol{w}_{\mathrm{B}_1}^{\mathrm{T}},\cdots,\boldsymbol{w}_{\mathrm{B}_{b-1}}^{\mathrm{T}}]. \tag{25}$$

Then, each batch of mismatched filter weights is obtained by

$$\begin{aligned}\boldsymbol{w}_{\mathrm{B}_i}^{\mathrm{T}}=-\lambda\Bigg[&\sum_k c\boldsymbol{S}_i(k)\boldsymbol{S}_i^{\mathrm{H}}(k)-\lambda\boldsymbol{s}_{\mathrm{ref}_i}(k)\boldsymbol{s}_{\mathrm{ref}_i}^{\mathrm{H}}(k)\\&+\lambda\varepsilon^2\boldsymbol{I}_{N_{\mathrm{B}}}\Bigg]^{-1}\boldsymbol{s}_{\mathrm{ref}_i}(k),\ i=0,1,\ldots,b-1,\end{aligned} \tag{26}$$

where $\boldsymbol{I}_{N_{\mathrm{B}}}$ is an $N_{\mathrm{B}}\times N_{\mathrm{B}}$ identity matrix, and

$$\boldsymbol{S}_i(k)=\left[S(k+iN_{\mathrm{B}}),\ \cdots,S(k+N_{\mathrm{B}}-1+iN_{\mathrm{B}})\right]^{\mathrm{T}}, \tag{27}$$

$$\boldsymbol{s}_{\mathrm{ref}_i}(k)=\left[s_{\mathrm{ref}}(iN_{\mathrm{B}}),\ \cdots,s_{\mathrm{ref}}(N_{\mathrm{B}}-1+iN_{\mathrm{B}})\right]^{\mathrm{T}}. \tag{28}$$

Then, the complex multiplication in solving Eq. (26) is $O[(2R+1)N\cdot N_{\mathrm{B}}+N\cdot N_{\mathrm{B}}(\log N_{\mathrm{B}}+1)]$. The original calculation is $O[(2R+1)N^2+N^2(\log N+1)]$. Usually, N_{B} is much smaller than N. Thus, the operation time of the batch version of the mismatched filter will decline sharply. Then the filter weights of the proposed algorithm are obtained.

5 Simulation results

To illustrate the performance of the proposed method, simulation results are presented. Suppose that three target echoes are received by the PBR system. The direct signal is collected by a low-gain reference antenna as a reference signal. The received signals are sampled and down-converted. The sampling frequency is 400 kHz, and the observation time is 0.2 s. The SNR in the reference signal is 10 dB. Parameters of the three target echoes are listed in Table 1.

Table 1 Simulation parameters of the three target echoes

Signal	SNR (dB)	Range (km)	Doppler frequency (Hz)
Target 1	−23	60.00	−192
Target 2	−30	90.00	166
Target 3	−15	26.25	243

Then, the matched and two mismatched methods are employed to obtain the detection results. Simulation results are shown in Fig. 5. To show the results clearly, the Doppler frequency is shown only from −1500 to 1500 Hz. For convenience, we call the mismatched filtering proposed by Wang et al. (2011) the original method and the improved method in this study the proposed method.

It can be seen from Fig. 5a that three targets exist. Due to range ambiguity, the range information cannot be extracted. It can be seen from Fig. 5b that the main lobe of the targets cannot be distinguished by applying the original mismatched filtering algorithm due to the low energy level in the reference signal. Fig. 5c shows that three targets are detected in the circles that are in accordance with the parameters listed in Table 1. Note that the mismatched filtering algorithm can suppress the range sidelobes to a certain extent but not fully. Thus, there are several sidelobes that are weaker than the main lobe. Then, the information of the target echoes can be extracted. In addition, assume that only one target exists in a single Doppler bin. Comparing the results of these two methods, we can conclude that the proposed method has a better suppression performance. In a PBR system, because of the low gain of the reference antenna or distant location of the transmitter, the reference signal may remain at a low energy level. With the decreasing energy level in the reference signal, the original mismatched filtering algorithm does not do well in sidelobe suppression. Thus, it is necessary to consider the energy level in the reference signal to improve the suppression performance.

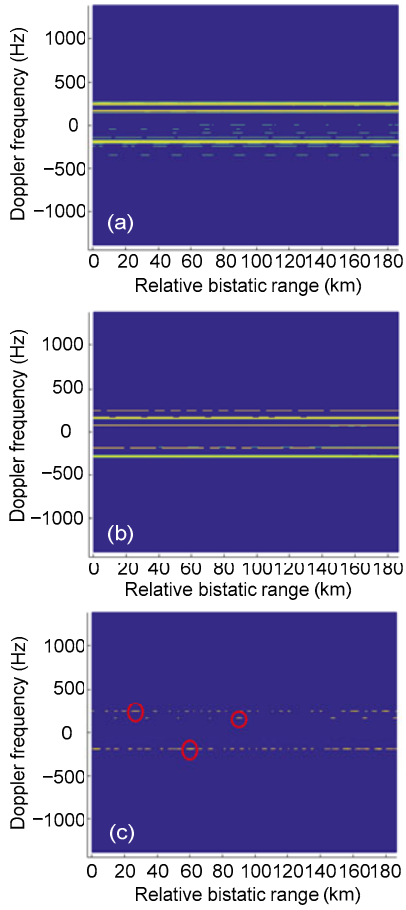

Fig. 5 Simulation results of the matched filter (a), the original method (b), and the proposed method (c)

6 Performances

In this section, the performances of the two algorithms are verified by simulation. The reference signal used to obtain the optimal weights is collected in a real environment. The sampling rate and observation time are 400 kHz and 0.2 s, respectively.

Due to the 64-μs line flyback, the spectrum of the ATV signal has high-level peaks every 15 625 Hz. It can be calculated that the ambiguity sidelobes in the range dimension are distributed the multiple of 64 μs/(1/f_s)=25.6 (except 0) bin away from the main lobe. Here, we suppose that f_s=400 kHz. For convenience, the repetition range bin of ambiguity range sidelobes

is 26. There are many range ambiguity sidelobes that need to be suppressed. It is almost impossible to realize the algorithm in practice. Indeed, when parts of the range ambiguity sidelobes are suppressed, others would be suppressed accordingly. So, we consider suppressing only four sidelobes in the range dimension to reduce the computation. Thus, the robust solution of the proposed method is given by

$$\boldsymbol{w}_{\mathrm{B}_i}^{\mathrm{T}} = -\lambda \left[\sum_{\substack{k=-2 \\ k\neq 0}}^{2} c\boldsymbol{S}_i(k)\boldsymbol{S}_i^{\mathrm{H}}(k) - \lambda \boldsymbol{s}_{\mathrm{ref}_i}(k)\boldsymbol{s}_{\mathrm{ref}_i}^{\mathrm{H}}(k) + \lambda\varepsilon^2 \boldsymbol{I}_{N_{\mathrm{B}}} \right]^{-1} \boldsymbol{s}_{\mathrm{ref}_i}(k). \tag{29}$$

The suppression performance and energy loss of these two methods with different values of c are shown in Fig. 6. Here, the suppression performance is defined as the energy difference of the first sidelobe between the matched and mismatched results. Similarly, the energy loss is defined as the energy difference between the matched and mismatched results. SNR in the reference signal is set to 15 dB compared with the energy level of the thermal noise.

Fig. 6a shows that the original method loses its suppression ability since the suppression performance remains unchanged with the increasing value of c. However, the suppression performance of the proposed method increases with the increasing value of c. These results show that the proposed method does well in ambiguity sidelobe suppression when the reference signal is at a low energy level. It can be seen from Fig. 6b that the energy losses of these two methods both increase with the increasing value of c, and that the values are basically the same. We can conclude from Fig. 6 that the original method loses its efficacy when the reference signal is at a low energy level, while the proposed method is not influenced.

To illustrate the relationship between the suppression performance and SNR in the reference signal, 100 independent trials are conducted to obtain the detection probability with different SNRs. SNR in the target echo is set to −20 dB and varies from 0 to 40 dB in the reference signal, to obtain the probability of target detection by applying two mismatched filtering methods. In particular, for each trial, when the SNR of the target echo is higher than 10 dB, the target is considered to be detected. Results are shown in Fig. 7.

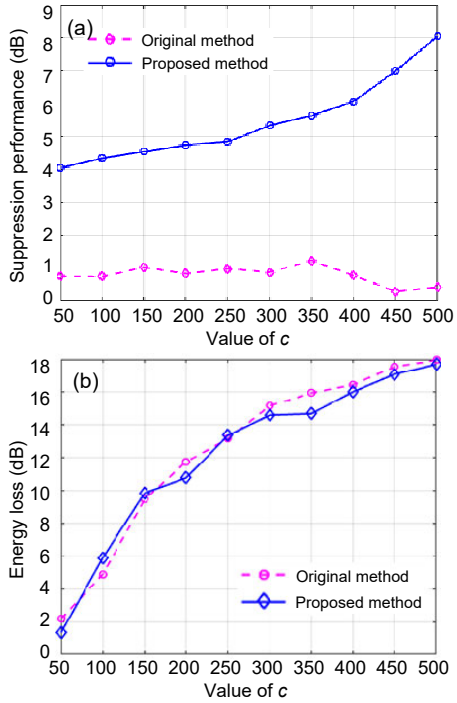

Fig. 6 Suppression performance (a) and energy loss (b) with different values of *c*

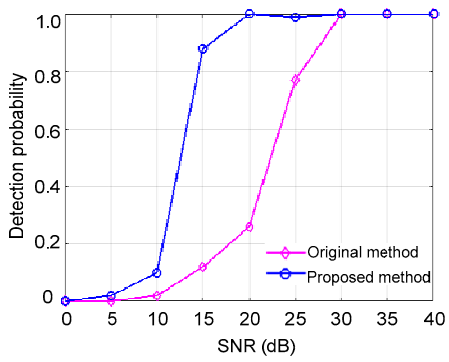

Fig. 7 Detection probability of the two methods

It can be seen from Fig. 7 that the detection probability of the proposed method is over 0.99 when the SNR in the reference signal exceeds 20 dB. When the detection probability of the original method exceeds 0.99, the SNR is no less than 30 dB. Due to the low SNR in the reference signal, the original method may lose its sidelobe suppression ability. More suppression is required to obtain lower sidelobe energy. Thus, the SNR loss in the main lobe increases and the SNR in the main lobe may be less than 10 dB. Thus, the target cannot be detected.

However, the proposed method can realize sidelobe suppression when a low SNR in the reference signal occurs. Thus, there is less SNR loss in the main lobe to obtain acceptable sidelobe energy. It can be concluded that the proposed mismatched filtering method has a higher detection probability than the original method when the SNR in the reference signal is lower than 30 dB. This proves the robustness of the proposed method.

7 Application on real data

To further demonstrate the effectiveness of the proposed mismatched filtering method, two methods are applied on real data obtained from an experimental PBR system. Fig. 8 shows the positions of the PBR system and ATV station in Shaanxi Province, China. Table 2 gives the parameters of the experimental system.

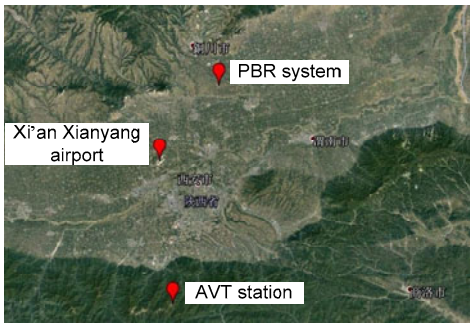

Fig. 8 Positions of the PBR system and ATV station

Table 2 Specific parameters of the experimental system

Station	Longitude (°)	Latitude (°)	Frequency (MHz)
ATV station	108.7921	33.8564	77.25
PBR system	109.6040	34.7308	
Airport	108.7642	34.4421	

Through digital beam forming, 15 beams are formed to cover the space area to be monitored. A separate antenna with low gain is used to collect the direct signal for clutter cancellation and mismatched filtering. Outputs with a duration time of 26 s from each beam are sampled by a digital receiving system with a sampling frequency of 400 kHz. Then, clutter cancellation is employed to remove the direct signal and multipath from the surveillance signal. After clutter cancellation, two mismatched filtering methods are applied. The outputs of the two methods are demonstrated in Fig. 9.

Before result analysis, note that the clutterers are usually not static due to wind speed and the unsatisfactory antenna. The clutterers usually consist of a little extension in the frequency spectrum. Thus, the clutterers cannot be canceled fully from the surveillance signal by applying the clutter cancellation algorithm. Therefore, there is clutterer residue in the results shown in Fig. 9.

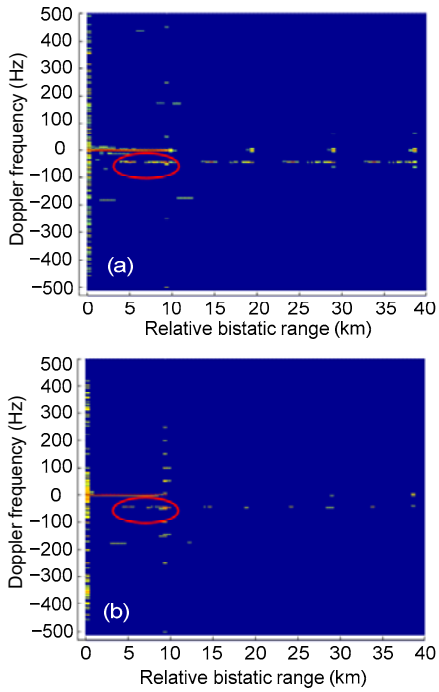

Fig. 9 Application results on real data: (a) original method; (b) proposed method

Fig. 9 shows that the target marked by circle is detected by applying both the original and the proposed mismatched filtering methods. However, it can be seen from Fig. 9a that the outputs of the original mismatched filtering method contain more ambiguity range sidelobes. Fig. 9b shows that the ambiguity range sidelobes are better suppressed by applying the proposed mismatched filtering method. It can be concluded that the ambiguity sidelobe suppression performance becomes poor due to the low SNR in the reference signal. Because this situation has been considered in the proposed method, the ambiguity sidelobe suppression performance is improved, which verifies the effectiveness of the proposed mismatched method.

8 Conclusions

In this study, we focused on the ambiguity sidelobe suppression problem in a PBR system when a low SNR reference signal is given. To address this problem, a robust mismatched filtering algorithm using worst-case performance optimization was proposed. In this proposed method, the optimal mismatched filtering solution was acquired by minimizing the sidelobe energy while limiting the SNR loss in the main lobe. In addition, the difference between the true and the observed reference signals was considered to obtain a robust solution. A batch version was employed to decrease the computational cost. Simulation results demonstrated that the proposed method has better sidelobes suppression performance when a lower SNR reference signal is given.

Application results based on continuous real data also verified the effectiveness of the proposed mismatched filtering method. In reality, the reference signal may remain at a low SNR level, which will invalidate the original mismatched filtering algorithm. To maintain the suppression performance, it is essential to consider the unpredictable energy level in the reference signal. According to the results based on real data, the proposed method retains its sidelobe suppression performance, whereas the original method loses its efficacy.

Contributors

Gang CHEN and Jun WANG designed the research. Gang CHEN processed the data and drafted the manuscript. Jun WANG helped organize the manuscript. Gang CHEN and Jun WANG revised and finalized the paper.

Compliance with ethics guidelines

Gang CHEN and Jun WANG declare that they have no conflict of interest.

References

Abdullah RSAR, Salah AA, Ismail A, et al., 2016. Experimental investigation on target detection and tracking in passive radar using long-term evolution signal. *IET Radar Sonar Navig*, 10(3):577-585. https://doi.org/10.1049/iet-rsn.2015.0346

Bok D, 2018. Reconstruction and reciprocal filter of OFDM waveforms for DVB-T2 based passive radar. Int Conf on Radar, p.1-6. https://doi.org/10.1109/RADAR.2018.8557339

Bournaka G, Ummenhofer M, Cristallini D, et al., 2017. Experimental study for transmitter imperfections in DVB-T based passive radar. *IEEE Trans Aerosp Electron Syst*, 54(3):1341-1354. https://doi.org/10.1109/TAES.2017.2785518

Chen G, Wang J, Guo S, et al., 2018. Improved mismatched filtering for ATV-based passive bistatic radar. *IET Radar Sonar Navig*, 12(6):663-670. https://doi.org/10.1049/iet-rsn.2017.0476

Clemente C, Soraghan JJ, 2014. GNSS-based passive bistatic radar for micro-Doppler analysis of helicopter rotor blades. *IEEE Trans Aerosp Electron Syst*, 50(1):491-500. https://doi.org/10.1109/TAES.2013.120018

Colone F, Cardinali R, Lombardo P, et al., 2009. Space-time constant modulus algorithm for multipath removal on the reference signal exploited by passive bistatic radar. *IET Radar Sonar Navig*, 3(3):253-264. https://doi.org/10.1049/iet-rsn:20080102

Colone F, Bongioanni C, Lombardo P, 2013. Multifrequency integration in FM radio-based passive bistatic radar. Part I: target detection. *IEEE Aerosp Electron Syst Mag*, 28(4): 28-39. https://doi.org/10.1109/MAES.2013.6506827

Garry JL, Baker CJ, Smith GE, 2017. Evaluation of direct signal suppression for passive radar. *IEEE Trans Geosci Remote Sens*, 55(7):3786-3799. https://doi.org/10.1109/TGRS.2017.2680321

Lorenz RG, Boyd SP, 2005. Robust minimum variance beamforming. *IEEE Trans Signal Process*, 53(5):1684-1696. https://doi.org/10.1109/TSP.2005.845436

Lu Y, Tan D, Sun H, 2007. Air target detection and tracking using a multi-channel GSM based passive radar. Int Waveform Diversity and Design Conf, p.122-126. https://doi.org/10.1109/WDDC.2007.4339393

Lv XY, Wang J, Wang J, 2015. Robust direction of arrival estimate method in FM-based passive bistatic radar with a four-element Adcock antenna array. *IET Radar Sonar Navig*, 9(4):392-400. https://doi.org/10.1049/iet-rsn.2014.0270

Ma H, Antoniou M, Stove AG, et al., 2018. Maritime moving target localization using passive GNSS-based multi-static radar. *IEEE Trans Geosci Remote Sens*, 56(8):4808-4819. https://doi.org/10.1109/TGRS.2018.2838682

Martelli T, Cardinali R, Colone F, 2018. Detection performance assessment of the FM-based AULOS® passive radar for air surveillance applications. 19th Int Radar Symp, p.1-10. https://doi.org/10.23919/IRS.2018.8448025

Milani I, Colone F, Bongioanni C, et al., 2018. WiFi emission-based vs passive radar localization of human targets. IEEE Radar Conf, p.1311-1316. https://doi.org/10.1109/RADAR.2018.8378753

Salah AA, Abdullah RSAR, Ismail A, et al., 2013. Feasibility study of LTE signal as a new illuminators of opportunity for passive radar applications. IEEE Int RF and Microwave Conf, p.257-262. https://doi.org/10.1109/RFM.2013.6757261

Tabassum MN, Hadi MA, Alshebeili S, 2016. CS based processing for high resolution GSM passive bistatic radar.

IEEE Int Conf on Acoustics, Speech and Signal Processing, p.2229-2233.
https://doi.org/10.1109/ICASSP.2016.7472073

Vorobyov SA, Gershman AB, Luo ZQ, 2003. Robust adaptive beamforming using worst-case performance optimization: a solution to the signal mismatch problem. *IEEE Trans Signal Process*, 51(2):313-324.
https://doi.org/10.1109/TSP.2002.806865

Wang HT, Wang J, Zhong LP, 2011. Mismatched filter for analogue TV-based passive bistatic radar. *IET Radar Sonar Navig*, 5(5):573-581.
https://doi.org/10.1049/iet-rsn.2010.0136

Yi JX, Wan XR, Li DS, et al., 2018. Robust clutter rejection in passive radar via generalized subband cancellation. *IEEE Trans Aerosp Electron Syst*, 54(4):1931-1946.
https://doi.org/10.1109/TAES.2018.2805228

Zaimbashi A, 2017. Target detection in analog terrestrial TV-based passive radar sensor: joint delay-Doppler estimation. *IEEE Sens J*, 17(17):5569-5580.
https://doi.org/10.1109/JSEN.2017.2725822

Zrnic B, Zejak A, Petrovic A, et al., 1998. Range sidelobe suppression for pulse compression radars utilizing modified RLS algorithm. IEEE 5th Int Symp on Spread Spectrum Techniques and Applications, p.1008-1011.
https://doi.org/10.1109/ISSSTA.1998.722532